


Droplet Generation in Standing-Surface-Acoustic-Wave Nebulization at Controlled Air Humidity

Mehrzad Roudini^{1,*}, Dennis Niedermeier,² Frank Stratmann,² and Andreas Winkler¹

¹Leibniz Institute for Solid State and Materials Research Dresden, Helmholtzstr. 20, 01069 Dresden, Germany

²Leibniz Institute for Tropospheric Research, Experimental Aerosol and Cloud Microphysics Department, Permoserstr. 15, 04318 Leipzig, Germany

 (Received 27 March 2020; revised 12 May 2020; accepted 26 May 2020; published 23 July 2020)

Surface-acoustic-wave (SAW) aerosol generators are very promising systems for applications requiring small aerosol sources and adjustable droplet-size distributions at low aerosol flowrates. However, the droplet-generation mechanism by SAW is yet unclear and dedicated experiments are necessary to gain further insights. In this work, the atomization zone is investigated experimentally to gain more insight into the droplet-generation mechanism by SAW. Three regions are observed in the atomization zone showing different acoustofluidic effects, including the formation of liquid films and patterns in a standing SAW (SSAW) wavefield and droplet generation. In addition, the influence of the humidity of surrounding air on the measured droplet-size distribution of the aerosols generated by SSW is investigated. Therefore, the air humidity is adjusted at constant air temperature in the sophisticated wind-tunnel Turbulent Leipzig Aerosol Cloud Interaction Simulator combined with an optical particle spectrometer with resolution down to the sub- μm scale. Besides the humidity influence on the droplet size in the measurement region, water-saturated air allowed us to estimate the initial droplet-size distribution at the atomization zone on the chip surface. This parameter is crucial for the determination of the underlying liquid-film disintegration mechanism, i.e., the droplets' origin. Hereby, a bimodal log-normal droplet-size distribution is obtained. The mean diameter of the main droplet fraction decreases from 7.2 to 5.3 μm with increasing relative humidity from 8.6 to 97%, apparently due to evaporation of smaller droplets in unsaturated air. A second peak corresponds to a mean diameter as small as 600 nm at high humidity conditions, which is likely to correspond to a droplet-generation mechanism not reported so far and extremely difficult to measure or visualize with conventional techniques. The droplet-size measurement results from the aerosol spectrometer are compared and validated in respect to existing droplet-generation models with the results of a phase-Doppler anemometry, a high-resolution, nonintrusive local aerosol-measurement technique.

DOI: [10.1103/PhysRevApplied.14.014071](https://doi.org/10.1103/PhysRevApplied.14.014071)

I. INTRODUCTION

Atomizers are attracting widespread interest in many technical processes due to their capability to disperse a bulk of a liquid into single droplets with different ranges in size and velocity, by means of the liquid kinetic energy or additional external forces. Small and compact surface-acoustic-wave (SAW) aerosol generators (or nebulizers) are able to generate micrometer-sized droplets with low velocity without the need for moving parts or nozzles, and were demonstrated as possible key components for various future applications, including inhalation therapy [1,2], material deposition [3–5], liquid chromatography and spectroscopy [6–8], and olfactory displays [9]. SAW aerosol generators operate by interaction of an acoustic wave excited on the surface of a piezoelectric substrate

with a liquid placed in its propagation path, a principle initially demonstrated by Kurosawa *et al.* [10], but only in recent years taken to an application-relevant technological level [11,12].

Despite the extensive diversity of demonstrated applications, only few studies have investigated the mechanisms underlying SAW aerosol generation [13,14], which is still not clear. In general, the estimation of the initial droplet-size distribution produced by aerosol generators in their atomization zone, i.e., at the orifice outlet or the SAW chip surface, is crucial for understanding the physics and the further development into application-adapted devices. In the case of SAW-based aerosol generation, the as-produced aerosols, however, have a narrow and highly dense plume and droplets in the low μm range. The measurement of such droplets is difficult due to their large number, rapidly changing droplet-size distribution with distance to the aerosol source due to evaporation, and spatially varying individual aerosol droplet velocities.

*m.roudini@ifw-dresden.de

The initial size of generated droplets can be estimated from the balance of capillary forces and vibration-induced forces in a liquid as done by previous researchers [13–16]. Firstly, Kelvin [15] introduced Eq. (1) to estimate the size D of pinched-off droplets based on low-frequency vibration processes (<1 MHz)

$$D \sim \lambda \sim \left(\frac{2\pi\sigma}{\rho f_c^2} \right)^{\frac{1}{3}}, \quad (1)$$

where σ and ρ are liquid-surface tension and liquid density, respectively, f_c is the frequency of the liquid-surface capillary waves, and λ is the wavelength of induced capillary waves by periodic vertical forcing. It should be noted that the liquid thickness is assumed to be appropriately larger than λ in this equation, an assumption not valid for standing-surface-acoustic-wave- (SSAW) based aerosol generation [11,14]. An important extension has been later established by Lang [16] considering the frequency of the capillary waves on the liquid surface one half the excitation frequency in ultrasonic atomization. Therefore, the size of disintegrated droplets from the liquid interface is given by Eq. (2)

$$D = k \left(\frac{8\pi\sigma}{\rho f^2} \right)^{\frac{1}{3}}, \quad (2)$$

where f is the excitation frequency, k is an experimental coefficient defined to be 0.34 based on Lang's experimental results, initially. However, when the exciting frequency is high (>10 MHz), as for SAW atomization, the physical behavior of the free surface of a drop does not correspond to the subharmonic relation ($f_c = f/2$). Instead, Qi *et al.* [13] suggested two existing capillary resonance frequencies on the liquid surface due to internal viscous attenuation ($f_c \sim \sigma/\mu R$) and inertial forces of the liquid film ($[f_c \sim (\sigma/\rho R^3)^{1/2}]$), where R is a characteristic length scale [13] for high-frequency SAW atomization. Their experimental and numerical investigations on a finite-thickness film surface showed the viscous-capillary resonance frequency as appropriate capillary resonance frequency, which can be used in Eq. (1) to estimate ejected droplet size. Equation (3) has been proposed by Qi *et al.* [13] from a viscous-capillary force balance to predict the liquid-instability wavelength

$$D \sim \frac{\sigma H^2}{\mu f L^2}, \quad (3)$$

whereas f is the SAW frequency, μ is the dynamic viscosity and H and L are characteristic height and length scales of the parent liquid film or drop, respectively. It was shown that H is related to the wavelength of the sound-waves generated in the liquid film due to the leaky SAW

and L is associated with the transferred mechanical power emitted by the SAW in the liquid. Later, Collins *et al.* [14] derived a modified Eq. (4) to estimate the ejected droplet size for a range of applied powers (2.6–10.2 W) and frequencies (26–131 MHz) suggesting that the ejected droplet sizes scale linearly with $We^{2/3} f^{-1}$ [14].

$$D \sim \frac{\sigma H^2}{\mu L^2} \frac{We^{\frac{2}{3}}}{f}, \quad (4)$$

where the acoustic Weber number $We \equiv \rho(\xi_o\omega)^2 L/\epsilon\sigma$ thereby captures the relative contributions from inertial forces and the stabilizing capillary stresses ξ_o is the vertical SAW displacement amplitude, ω is the SAW angular frequency, L is twice the SAW wavelength, and $\epsilon \equiv H/L$.

For liquid-surface instability and droplet generation in SAW atomization, very important parameters are the thin liquid-film shape and the geometry and placement of the liquid source, i.e., the fluid supply. The interaction between the liquid flowing from its source with the excited SAW forms the resultant liquid-film pattern outside and inside the acoustic wavefield. Therefore, various process parameters including liquid properties, surface chemistry, local SAW wavelength and amplitude, and local SAW configuration (traveling and standing wave, SAW polarization) govern the spreading and shape of the SAW-induced and stabilized liquid film on the chip surface. While the existing experimental data in the literature concentrates on traveling surface-acoustic-wave configuration, in this work, the experimental measurement of the geometries of the liquid film during atomization has been performed with the more spatially defined and reproducible standing SAW configuration, as explained in the next section, where we discuss our findings with respect to existing data and models. Besides the model predictions, here, SAW-generated aerosol droplets are measured by various techniques including laser diffraction [11,14,17] and phase-Doppler anemometry (PDA) [10,18]. In the probably most detailed study so far, Collins *et al.* [14] measured SAW-generated droplet-size distributions using laser diffraction shown in the results section. The mass median droplet diameter (MMD) of two peaks observed in the droplet-size distribution was measured for different experimental conditions and showed a linear relationship with $(\epsilon We)^{2/3} f^{-1}$.

Previous studies also revealed that air humidity has a significant influence on the measured droplet-size distributions. For instance, some studies have been proposed that a high concentration of water vapor in humid air may reduce the evaporation rate and lead to an evaporation-condensation equilibrium, which maintains the droplet-size distribution from the aerosol source to the measurement position downstream the atomizer [19,20]. Although, it should be borne in mind that existing results were obtained utilizing different droplet-size measurement

techniques with different droplet-size range resolutions and at various measurement locations.

In the current study, the atomization zone is experimentally visualized by high-speed video microscopy to gain insight into the droplet-generation mechanism by SSAW. Moreover, the so far furthest developed compact SAW aerosol generator was investigated inside the Turbulent Leipzig Aerosol Cloud Interaction Simulator (LACIS-T, [21]), a large turbulent wind tunnel, at different constant levels of air humidity in order to determine the initial droplet-size distribution and to get a closer view on the underlying droplet-formation mechanisms on the chip surface. The results are compared to droplet-size measurements in ambient air acquired using phase-Doppler anemometry and with previously reported droplet-size data and droplet-generation models.

II. EXPERIMENT

A. SSAW aerosol generator

The aerosol generator in this study utilizes standing surface acoustic wave to disintegrate an acoustically stabilized liquid film with a thickness on the order of the SAW wavelength to micrometer-sized droplets without macroscopically moving parts or nozzles [11,14]. A schematic of its main components is shown in Fig 1. A custom computerized numerical control (CNC) milled and anodized aluminum platform is used as the chip holder, comprising cooling fins on its bottom side for efficient heat dissipation, e.g., for the event of temporary absence of fluid in the propagation path, a cavity on the top side for placement of heat-conductive foil and the SAW chip, and alignment features. The customized printed circuit board (PCB, manufactured by Würth Electronic GmbH & Co. KG., Germany) comprises strip lines matched to 50 Ω impedance, female SMA PCB connectors and gold-coated spring pins, which directly contact the pads on the chip surface. Partially open microfluidic channels and interdigital transducers are structured on a 4" single-side polished

lithium niobate wafer substrate with X -propagation direction ($128^\circ\text{YX LiNbO}_3$), subsequently diced into single SAW aerosol-generation chips ($8 \times 19 \text{ mm}^2$). In the current chip layout, two interdigital transducers (IDT) ($\lambda/4$ type, $90\text{-}\mu\text{m}$ wavelength, 46 electrode pairs, 0.5-mm aperture, matched to $50\text{-}\Omega$ impedance by the number of finger electrodes) are opposing each other with a distance of 6 mm for SSAW excitation based on superposition of two counterpropagating traveling SAWs.

The IDTs consist of subsequent layers of Ti (5 nm) and Al (295 nm) and are prepared via electron-beam evaporation and lift-off technique. A $1\text{-}\mu\text{m}$ -thick SiO_2 layer is rf sputter deposited onto the surface of the wafer to prevent electrode corrosion. The electrical contact pads are opened by Ar ion etching. Finally, a $50\text{-}\mu\text{m}$ -thick SU-8 layer is deposited to the substrate surface via spin coating and structured via double-exposure photolithography to create microfluidic channels for the fluid supply (for more information refer to Ref. [11]). These structures are designed in a droplike geometry to enable a sufficient mechanical stability and to reduce the effective polymer cross section in the acoustic beam at the same time. The channel outlets are placed in the chip center at the very boundary of the acoustic beam, a location determined by laser-Doppler vibrometry measurements (UHF120, Polytec GmbH). High-frequency signals are supplied at the operation frequency of the IDTs, approximately 43 MHz , corresponding to the $|S_{11}|$ minima via SMA cables from a dual-channel PowerSAW signal source (PSG, BelektroniG GmbH, Germany) with an electrical forward power of 2.1 W for each IDT. A nEMESYS 290N laboratory syringe pump (Cetoni GmbH) is used as a fluid source and connected to the microchannels via sealing rings, a PEEK block with drilled holes and PTFE tubing. DI water is used for the aerosol generation and the liquid flow rate is $100 \mu\text{l}/\text{min}$ during all droplet-size measurements.

The disintegrated droplets from the thin liquid film and atomization zone have been visualized using a high-speed video camera (Phantom VEO 410, Vision Research Inc.)

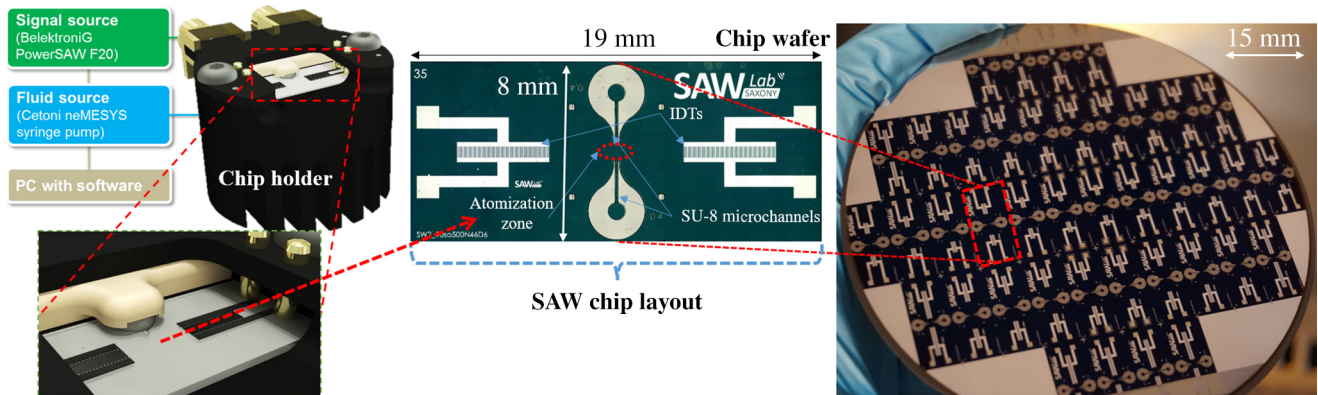


FIG. 1. Schematic of the compact SAW aerosol generator and the used SAW chip layout.

connected to a long-distance microscopic lens (OPTEM) with 18x magnification in order to provide more clues of existence of submicron droplets.

B. Wind-tunnel and optical particle spectrometer

The assembled SAW aerosol generator was mounted inside the turbulent moist-air wind tunnel LACIS-T [21] at Leibniz TROPOS [see Fig. 2(a)]. LACIS-T is a closed-loop wind tunnel of the Göttingen-type in which the air circulates continuously with a total flowrate of up to 12.000 l/min. It is intentionally designed to study turbulent cloud interaction processes at typical cloud conditions including warm, mixed-phase, and cold clouds. The cloud investigations are conducted in the measurement section of LACIS-T, which is of cuboidal shape, 200 cm long, 80 cm wide, and 20 cm deep [see Fig. 2(b)]. Clouds can be formed in the measurement section via turbulent mixing of three individual conditioned flows (i.e., two particle-free air flows, and one aerosol flow).

The LACIS-T setup and operating principle are briefly explained in the following (a detailed description is given in Ref. [21]). Two radial blowers separately drive the two air flows. Each flow passes a particle filter (Filter class U16) afterwards. Each particle-free air flow can then be humidified in the humidification system consisting of three Nafion® tubes per flow branch. The Nafion® tubes are surrounded by temperature-controlled water jackets. Water diffusion takes place through the Nafion® tubes into the

particle-free air flows so that the dew-point temperature measured behind the humidification system is equal to the temperature of the water jacket. Note that the humidification system can also be bypassed allowing investigations under dry conditions. Afterwards, these two (humidified) air flows are turned around and enter the heat exchangers, where both flows are individually tempered. Both air flows then pass a passive turbulence grid (mesh length of 1.9 cm, rod diameter 0.5 cm, and a blockage of 30%), which is situated 20 cm above the measurement section. At the inlet of the measurement section, the two conditioned particle-free air flows are combined and turbulently mixed, resulting in a well-defined turbulent flow. In the mixing zone, aerosol particles can be injected for cloud-interaction studies (not done in this study). After passing through the measurement section, the entire flow is dried, split up again into two air flows, and the whole procedure starts again. The initial temperature and dew-point temperature can be adjusted between room temperature and $-40\text{ }^{\circ}\text{C}$ with an accuracy of $\leq 0.1\text{ K}$. In consequence, the mean relative humidity can be adjusted in a range between approximately 1% and $>100\%$.

The SAW aerosol generator is positioned inside the measurement section, in center position and 40 cm below the air inlet. An optical particle spectrometer (welas® 2300 aerosol sensor, PALAS GmbH, Germany) is positioned 10 cm below the SAW aerosol generator to determine the size distribution of the generated particles and droplets [Fig. 2(c)]. The measuring principle of the aerosol

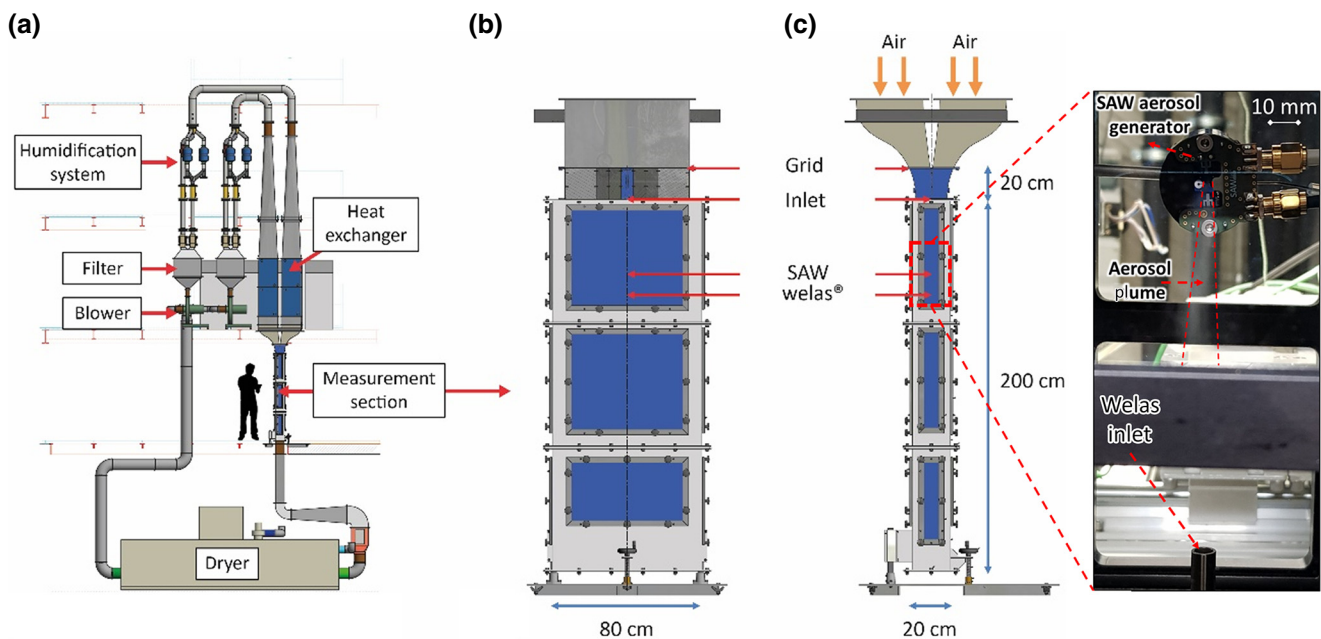


FIG. 2. The moist-air wind tunnel LACIS-T inside the TROPOS Cloud Laboratory: (a) schematic representation of the wind tunnel inclusive main components, and (b) schematic representation of the measurement section inclusive main components, and (c) schematic representation of the measurement section including the position of the SAW aerosol generator and the welas® 2300 aerosol sensor marked by the red arrows. (Schematic copyrights: Ingenieurbüro Mathias Lippold, VDI; TROPOS).

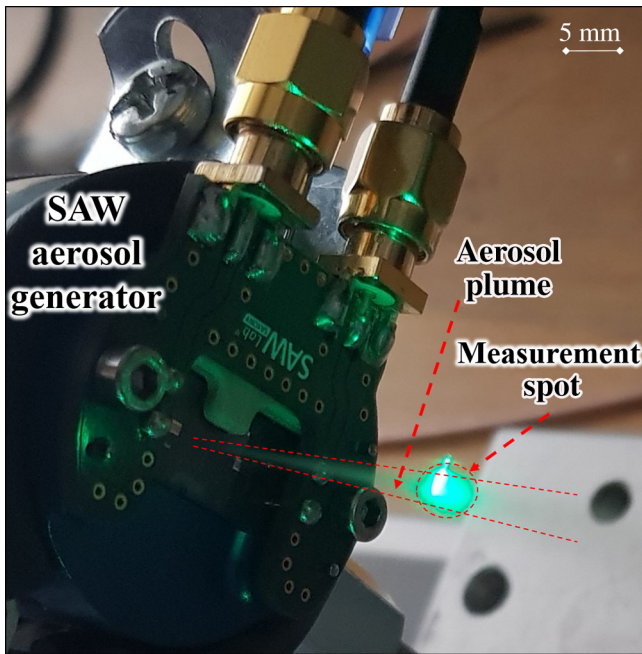


FIG. 3. Droplet-size measurement setup using PDA. Water with a flowrate of a $100 \mu\text{l}/\text{min}$ and an electrical forward power of 2.1 W for each IDT have been used during aerosol measurements.

spectrometer is based on scattered light analysis of individual particles.

A constant volumetric flow of $5 \text{ l}/\text{min}$ passes through the spectrometer. Inside welas® 2300, a white light source illuminates a T-shaped measuring volume, where each particle generates a scattered light pulse. The height and intensity of this light pulse is a measure for the particle diameter. The particle concentration is determined from the number of pulses detected within a certain time frame and the known measurement volume and flowrate. For each dew-point temperature, particle detection took place over a time frame of 5 min . The obtained results are presented in the next chapter. Also, see Supplemental Material [22] for the experimental setup using the SAW aerosol generator inside the turbulent moist-air wind tunnel LACIS-T.

In this study, the volumetric flow of both particle-free air flows is set to $4.4 \text{ m}^3/\text{min}$ resulting in a mean velocity of $1.4 \text{ m}/\text{s}$ in the measurement section. The initial temperature and dew-point temperature is the same for both particle-free air flows. Multiple experiments are performed whereby the dew-point temperature is set to different levels, i.e., $-14 \text{ }^\circ\text{C}$, $10 \text{ }^\circ\text{C}$, $15 \text{ }^\circ\text{C}$, $18 \text{ }^\circ\text{C}$, and $20 \text{ }^\circ\text{C}$, and the temperature of both particle-free air flows is held constant at $20.5 \text{ }^\circ\text{C}$. The humidity and the dew-point temperature are varied in random order. The order of the runs in the experiment is $T_d = 18 \text{ }^\circ\text{C}$, $T_d = 10 \text{ }^\circ\text{C}$, $T_d = 15 \text{ }^\circ\text{C}$, $T_d = -14 \text{ }^\circ\text{C}$, $T_d = 20 \text{ }^\circ\text{C}$. Consequently, the mean relative humidity is varied between 8.6% and 97% .

To monitor the settings, measurements of dew-point temperature (MBW 973 dew-point mirror, MBW, Switzerland) and temperature (Pt100 resistance thermometer, TC Meß- und Regeltechnik GmbH, Germany) are performed in each flow branch at the inlet of the measurement section.

C. Phase-Doppler anemometry

In addition to the measurements in LACIS-T, a study with phase-Doppler anemometry, a nonintrusive local aerosol measurement technique, is carried out at normal ambient conditions. In PDA, the phase difference of the Doppler frequencies measured by multiple detectors located at different angles delivers the size of individual droplets. In the present study, a one-component measurement is performed by a PDA (Dantec Dynamic A/S, Denmark) based on conventional optics, and a signal processor is used to characterize the velocity field and sizes of spherical particles downstream of the atomizer. PDA optical settings are similar to the settings used in a previous study [23]. The measurement location is set along the centerline at around 24 mm from the chip surface to avoid common complication in the droplet-size measurement due to the high density of the aerosol plume in the vicinity of the atomizer [Fig. 3]. A total of at least 4000 individual droplets are acquired within a time limit set at 30 s . The maximum uncertainty on the droplet velocity and diameter measurements are both $\pm 2\%$ and the maximum tolerance for the sphericity validation is 10% .

III. RESULTS AND DISCUSSIONS

A. Atomization zone observation

The atomization zone is optically visualized to gain more insight into the hydrodynamics associated with SSSAW interaction with a microchannel-introduced liquid film, besides, droplet generation from developed liquid patterns. A microscopy image of the used atomization chip with two IDTs and microchannels is shown in Fig. 4(a). Only one of the microchannels is used for the current study to have better optical accessibility to the atomization zone. A high-speed image of the atomization zone in front of a $30\text{-}\mu\text{m}$ height microchannel is shown at Fig. 4(b). As observed, a liquid film with chaotic surface fluctuations is immediately formed due to the contribution of Eckart streaming (region 1), at the edge of the acoustic wavefield. The observed extended film is similar to a front-running film region observed by Collins *et al.* [14]. As seen in Fig. 4(c), a thinner liquid film is formed following the initially extended liquid film and advances perpendicular to the main SAW propagation direction and towards higher amplitudes into the atomization zone (region 2). It is worth discussing these interesting facts in comparison to investigations of Rezk *et al.* [24] on liquid films under acoustic excitation. Local dewetting spots can be observed in a

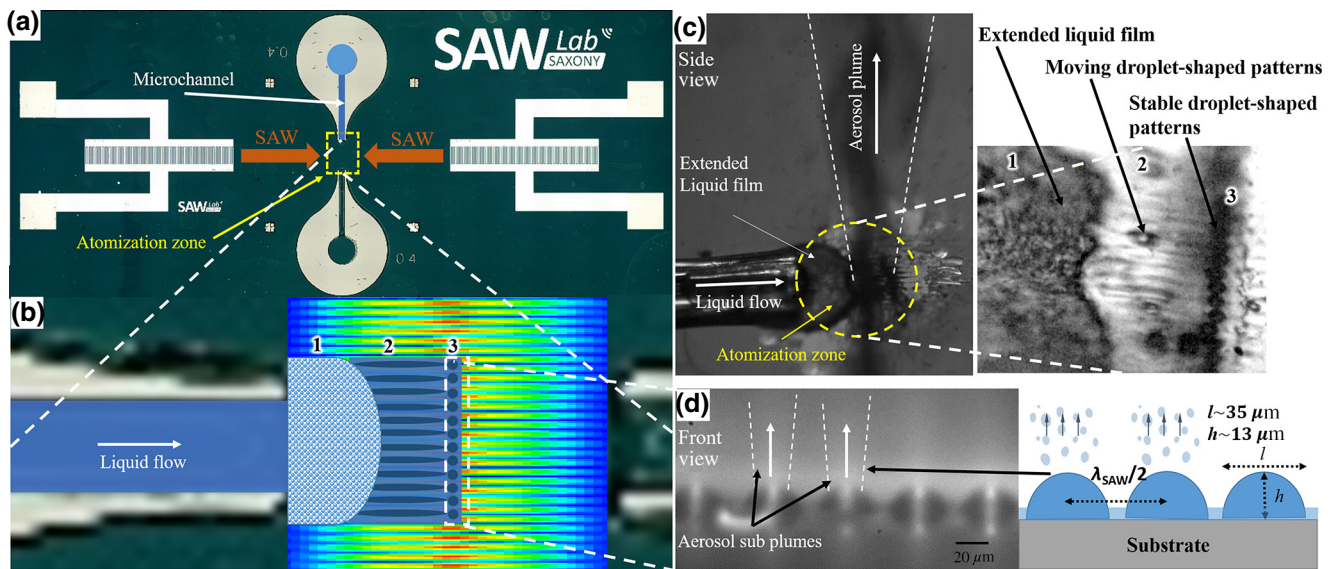


FIG. 4. (a) Microscopy image of SAW chip for aerosol generation with microchannels integrated in droplike SU-8 polymer structures, located outside of the acoustic aperture, i.e., in the boundary region of the acoustic beam. (b) Schematic of observed different liquid-film regions during liquid atomization in the region of the SSAW wave field as well as illustrated SAW amplitude distribution in front of the microchannel outlet. Microscopy image of the atomization zone and an extended thin liquid film in front of the microchannel (c) side view and (d) front view.

height-modulated film depending on wettability properties of the liquid and the SSAW displacement velocity distribution. Since the thickness of the thin discharging film seems to be fairly smaller than the sound wavelength in water (approximately $33 \mu\text{m}$, smaller than $\lambda_{\text{SSAW}} = \lambda_{\text{SAW}}/2$), it seems to be insufficient to support the formation of bulk sound waves. Accordingly, Rayleigh streaming driven by a weak convective mechanism (Stokes drift) dominates here over Eckart streaming.

Another observed acoustofluidic phenomenon is oscillating droplet-shaped patterns, which are generated and traveled frequently on the modulated liquid film (region 2). Recently, this phenomenon is reported in the literature as a solitonlike wave pulse propagation using traveling SAW, which grows mainly from the capillary ridges above the advancing film [24]. It seems, once the liquid film exists on a wavefield region with a certain amplitude displacement, the film local fluid volume reaches a critical value, as a consequence, liquid droplet-shaped patterns dominated by Eckart streaming are formed and displaced.

Moreover, SSAW-induced quasistable liquid droplet-shaped patterns are observed interestingly at the location with highest SSAW amplitudes (region 3) during the atomization process [shown in at Fig. 4(c)]. The observed patterns formed periodically in a distance of the half of the SAW wavelength $\lambda_{\text{SAW}}/2$, which are shown clearly in front view of the atomization zone [Fig. 4(d)]. From the Fig. 4(c), it is clear, that almost all droplets corresponding to the main droplet plume originate from the highlighted atomization zone consisting of regions 2 and 3.

The high-speed images from front and side views, shown in Figs. 4(c) and 4(d), provide compelling evidence that resultant droplets originate entirely as aerosol subplumes from observed individual droplet-shaped liquid patterns in the SSAW wavefield. See Supplemental Material [25] for an overview on the atomization zone with periodic, spatially separated, droplet-shaped liquid patterns established and stabilized by the acoustic wave field, which are disintegrated into vertically directed aerosol clouds, the aerosol subplumes.

The liquid-pattern geometries in region 3 with the characteristic length (l) and height (h) are measured using image processing for different electrical input powers and liquid flowrates. See Supplemental Material [26] for a high-speed video microscopy recording showing the front view of the atomization zone at higher magnification for different liquid flowrates. As seen in Fig. 5(a), increasing the flowrate has no significant influence on the liquid-pattern characteristic height, however, increasing electrical power slightly reduced the liquid-pattern height from 14.9 to $12.5 \mu\text{m}$. The liquid-pattern height in the middle of the wave field equals $h \sim 13 \mu\text{m}$ ($\sim 3/8\lambda_v$), which is smaller than the thin advancing film height observed by Collins *et al.* ($h \sim 7/8\lambda_v$) [14]. λ_v is the vertical component of the SAW-induced longitudinal pressure wave in the liquid. Moreover, Fig. 5(b) shows that the liquid-pattern characteristic length (l) seems to be unaffected when the electrical power and liquid flowrate are increased. Therefore, the liquid pattern length (l) in the middle of the wave-propagation path seems to equal $l \sim 35 \mu\text{m}$. Consequently, according

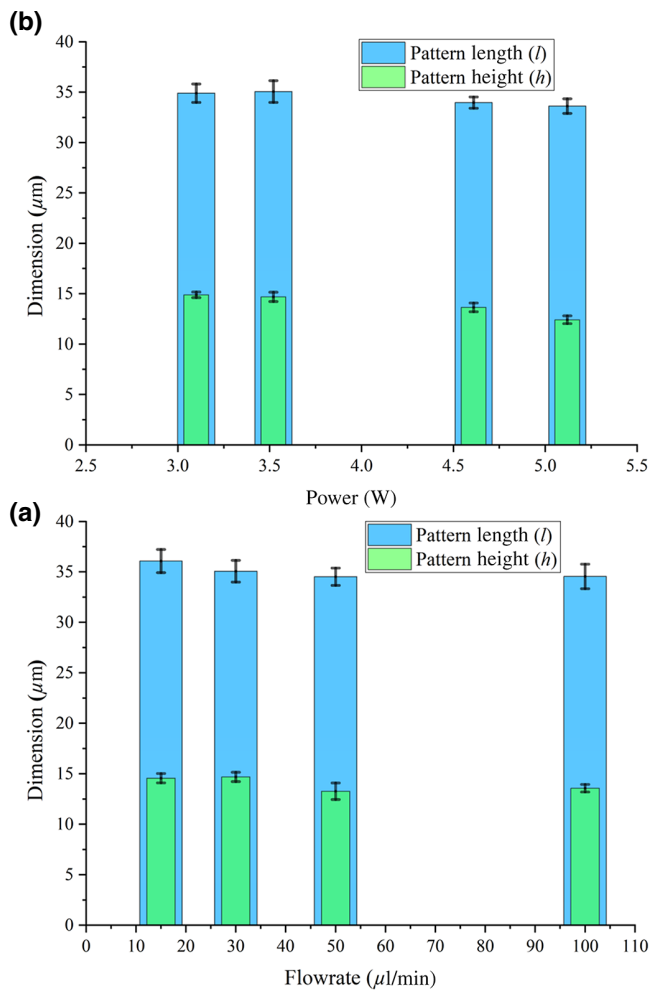


FIG. 5. Dependence of the experimentally measured local height (h) of the liquid patterns on (a) the liquid flowrate and (b) input SAW power. Dependence of the width (l) of the liquid patterns on (a) the liquid flowrate and (b) input SAW power. Error bars represent a standard deviation of the measured parameter between ten different captured images taken at each operation condition.

to our measurements it is necessary to change liquid-film configuration of previous models to predict accurately the initial size of generated droplets using SAW atomization.

B. Particle- and droplet-size distribution

The particle- and droplet-size distributions measured at five different dew-point temperatures are shown in Fig. 6(a). In all cases, a multimodal distribution with droplet diameters below $30 \mu\text{m}$ is observed. Moreover, the number of measured droplets is increasing considerably with increasing relative humidity of air flow in the wind tunnel. This effect is expected considering droplet evaporation in unsaturated air. The influence of the relative humidity on the liquid-surface tension is neglected in a first approximation. The first peak appears at a mean

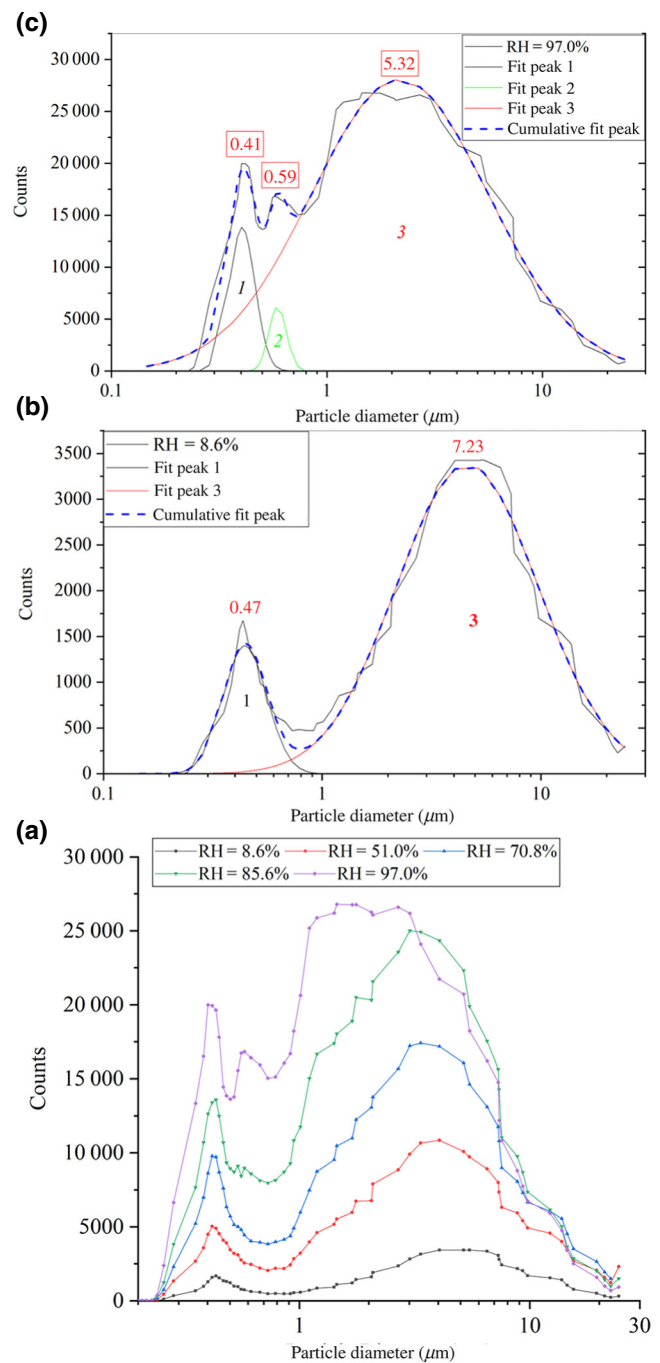


FIG. 6. (a) Particle- and droplet-size distributions measured by welas® 2300 for five different inlet dew-point temperatures T_d leading to five different values of relative humidity inside the measurement section of LACIS-T (8.6, 51.0, 70.8, 85.6, and 97.0%). The counted particle and droplet number per size bin is plotted versus the particle diameter. Log-normal distribution curve fitting approach shown for (b) RH = 8.6% and (c) RH = 97.0%.

diameter of about 400 nm and mainly changes in terms of droplet number but not in terms of mean diameter. However, it should be noted that 400 nm is about the

droplet-size measurement resolution of the welas® 2300 aerosol sensor. This is well below the resolution limit of other techniques including PDA and laser diffraction, but here could result in the disregard of even smaller droplets. Therefore, we concentrate on the discussions of the main peak.

The mean diameter of the main droplet peak is located at around 6 to 8 μm and decreases with increasing dew-point temperature. This counterintuitive behavior can be explained by the fact that the formed small droplets rapidly evaporate with decreasing relative humidity. Thereby, the total droplet number decreases and the shape of the measured size distribution shifts towards larger droplet sizes due to the relatively faster evaporation of smaller droplets. In all scientific SAW atomization studies reported so far, the generated droplets are analyzed in normal lab atmosphere, i.e., approximately 20–25 $^{\circ}\text{C}$ and 50% humidity, in a distance of several cm to the atomization zone, leading to shifted droplet peaks and possible misinterpretation of the underlying physics [1,10,14].

The peak fitting approach used here is based on the superposition of up to three log-normal distribution functions to the measured droplet number density distribution [shown in Figs. 6(b) and 6(c) for RH = 8.6% and 97.0%]. The fit peaks of peak 1 and peak 3 (main peak) are presented with a black and red color, respectively. After a profound data analysis, a small peak (peak 2 in green color) seems to appear at a mean diameter of about 600 nm during aerosol generation at high-humidity conditions [Figs. 6(a) and 6(c)]. Its observation can be again described by increasing evaporation of small droplets with decreasing relative humidity. Therefore, this peak would be less pronounced and would even disappear at dryer air conditions. However, it should be considered that generated aerosols are not homogeneous, and that the core of the aerosol plume may have a higher relative humidity compared to the surrounding air stream. This may lead to the survival of very small droplets even at a lower value of relative humidity set in the wind tunnel.

The log-normal mean diameter and its standard deviation are used to compare the influence of relative humidity. The measured log-normal mean diameter variations of peak 1 and peak 3 with varying relative humidity at otherwise constant experimental conditions are depicted in Fig. 7(a). As observed, an increase of relative humidity from 8.6 to 97% leads to about 26% decrease in the mean droplet size of the main droplet fraction. The possible source of the small particles in peak 1 is discussed in detail in the next sections. Figure 7(a) shows a comparison between droplet-size measurement results from the current study and existing theoretical and experimental equations [Eqs. (1)–(4)] adapted to the atomization conditions used in this study. According to the derived theoretical equation by Lang [Eq. (2)] for ultrasonic atomizers with subharmonic half-excitation-frequency relationship, the

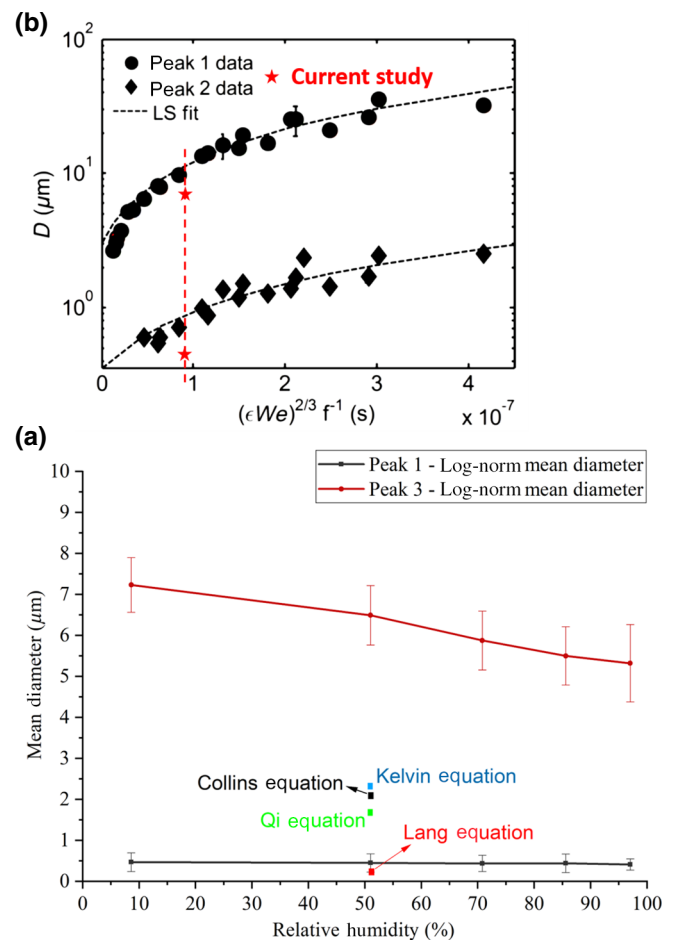


FIG. 7. (a) Effect of relative humidity (RH) on the log-normal mean droplet size for the main peak, first peak, and their standard deviations. (b) Linear relationship between experimental measured MMD for two observed peaks and $(\epsilon We)^{2/3} f^{-1}$ [14].

estimated average droplet size is much smaller than our measured droplet size corresponding to the main peak. The defined assumption that the frequency of the capillary waves on the free surface is one half of the excitation frequency, which is far below that used in the current study may lead to this difference. Moreover, if the viscous-capillary resonance frequency is chosen as appropriate capillary resonance frequency for high-frequency surface-acoustic-wave atomizers, as Qi *et al.* suggested [13], Eqs. (1), (3), and (4) also lead to a mismatch of the calculated and measured mean droplet size linked to the main peak. A likely reason is a resulting smaller characteristic height and length of the thin liquid film resulting from microchannels used in this study compare to their initial liquid source height as explained in the previous section. Therefore, there is no proper model explaining the current droplet size generated by SAW-based atomizers.

Interestingly, despite of the deviation between measured droplet size and existing theoretical equations, the

measured aerosol size of peak 1 and peak 3 from the current study agree well with the previous suggestion by Collins *et al.* [14], that the ejected droplet sizes scale linearly with $(\epsilon We)^{2/3} f^{-1}$ shown in Fig. 7(b). However, it should be borne in mind that the influence of the characteristic height on the mean droplet size is eliminated in these results. This is even more interesting, considering the use of traveling SAW and a fluid supply in the SAW beam path in the study of Collins *et al.* [14] versus standing SAW and a fluid supply at the beam boundary in this study. The mechanism of droplet generation may be principally similar for both, very different setups.

The results from the two measurement techniques, aerosol spectrometer and PDA, are compared in Fig. 8. It should be noted here that the measurement location of PDA and welas aerosol spectrometer are around 24- and 100-mm distance from the chip surface. The size distribution measured by PDA locally in the aerosol beam shows a main peak mean diameter of $7.35 \mu\text{m}$ and that from welas had a main peak mean diameter of $6.49 \mu\text{m}$. The averaged droplet size corresponding to the main peak measured by two different techniques with slightly different measurement conditions showed reasonably comparable results. Furthermore, it is observed that peak 1 is not entirely detected by PDA measurement technique. Since the measured particle-size range of peak 1 is lower than the PDA resolution limit, PDA seems not to be capable of measuring existing nanoscale droplets. The origin of such small mist is not revealed yet and it needs more comprehensive investigations.

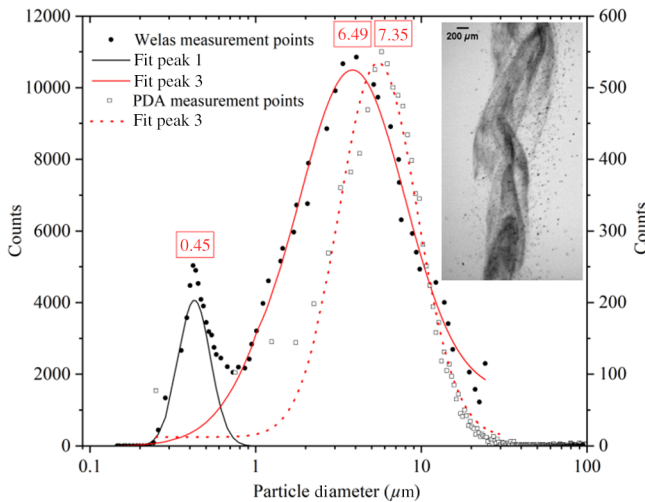


FIG. 8. Comparison of particle- and droplet-size distributions using PDA (at approximately 20°C and 50% RH) and aerosol spectrometer ($\text{RH} = 51\%$). Visualization of the ejected droplets during SAW atomization using a high-speed video camera (10,000 fps with $100 \mu\text{s}$ exposure time) proves two different droplet-size ranges indicated as two separate peaks in the measured droplet-size distribution.

The measured particle-size distribution plot suggested two different atomization mechanisms are involved during SAW interaction with the discharged liquid film. As Fig. 8 reveals, the generated droplet plume using a SAW atomizer consists of an obvious droplet-size range around $10 \mu\text{m}$ beside a mist of droplets smaller than $1 \mu\text{m}$ in the background. Regarding the observed mist, one possible and likely explanation could be a droplet generation by high-speed microjets induced by the collapse of cavitation bubbles inside the liquid film [27,28]. According to the previous literature, a frequency of approximately 10 MHz constitutes a limit above which microcavitation seems unlikely to occur [29]. However, SSW aerosol generation is the result of a highly resonant acoustofluidic interaction in a thin fluidic film, and strong pressure changes can occur in such a setup on very small timescales, which may be able to initiate cavitation. In a first approximation, considering the current SAW-based atomizer working frequency (43 MHz), a 0.5-mm -sized aperture, a 0.5-mm -sized length of the atomization zone area (A) in propagation direction and an input ac signal power of 4 W , an approximate acoustic pressure amplitude within the fluidic pattern of about 36 bar seems realistic. The amplitude of the pressure field is roughly estimated by $P_o = \sqrt{2W\rho c/A}$ with the applied power (W), density of medium (ρ), and the speed of the sound in medium (c) [29]. The transmitted acoustic pressure from the substrate into the liquid is estimated using the incident pressure transmissivity equation $\{(P_{o2}/P_{o1}) = [2r/(r+1)]\}$, where r is the impedance ratio $[r = (\rho_2 c_2 / \rho_1 c_1)]$ at the boundary, which seems to be principally sufficient to drive cavitation, compared with the threshold pressure ($P_{\text{Threshold}} \sim 16 \text{ bar}$) calculated by $P_{\text{Threshold}}^{1.67} = 0.06f$ [30] for the corresponding working frequency.

As the existence of cavitation is of fundamental importance, further investigations are necessary to prove its existence and its contribution to the droplet generation.

IV. CONCLUSION

In the current study, the behavior of the furthest developed SAW-based aerosol generator is investigated inside the LACIS-T wind tunnel at different constant levels of air humidity to determine the initial droplet-size distribution in SAW nebulization, and to get deeper insights in the underlying droplet-formation mechanisms on the chip surface. The adverse effect of the surrounding gas phase on the measured droplet-size distribution is confirmed, highlighting the importance of water-saturated gas atmosphere during droplet-size measurements. It is thus obvious, that the design of the aerosol generator and the aerosol guidance in a real-world application will determine the usable droplet size, as also determined by the local air humidity.

The results indicate a multimodal distributed droplet-size distribution with two main peaks and droplet diameters below 30 μm . A first peak appears at a mean diameter of about 400 nm and mainly changes in terms of droplet number with increasing dew-point temperature. However, droplets may be even smaller and not detectable with currently available measurement systems. The mean diameter corresponding to the main peak decreases with increasing relative humidity apparently due to evaporation of small droplets. After a profound data analysis, a third peak seems to appear at a mean diameter of about 600 nm during aerosol generation at high humidity conditions.

Furthermore, the atomization zone is optically inspected to visualize the droplet generation and the hydrodynamics in the acoustically generated and stabilized liquid film and the liquid patterns. A liquid film with chaotic surface fluctuations is immediately formed in front of the channel outlet and in the edge of the acoustic wavefield due to the contribution of Eckart streaming. Within the SAW wavefield, a thin modulated film is observed advancing perpendicular to the main SAW propagation direction and towards higher amplitudes into the atomization zone. The local droplet-shaped liquid patterns are generated and traveled frequently on the modulated liquid film. Moreover, SSAW-induced quasistable liquid droplet-shaped patterns are observed at the location with highest SSAW amplitudes during atomization process. Finally, the droplet-shaped liquid patterns seem to be the local origins of the resultant droplets using a SSAW excitation and a spreading liquid film from the microchannel.

In future, further experiments have to be carried out to understand better the physical phenomena underlying SAW atomization and the resulted droplet-size distribution and to prove the existence of cavitation, e.g., by high-resolution high-speed video microscopy or by showing typical damage pattern, and by investigation of the droplet-size distribution with the method used in this study at varied SAW wavelength and fluid flowrate.

ACKNOWLEDGMENTS

This work is supported by EFRE InfraPro project “ChAMP: Chip-based acoustofluidic Medtech Platform” and PDA droplet-size measurements are carried out in an industry-project financed by Thermofisher Dionex GmbH. We also acknowledge the members of the IFW clean room, the SAWLab Saxony, and the IFW workshop for chip and holder manufacturing.

[1] A. Qi, J. R. Friend, L. Y. Yeo, D. A. Morton, M. P. McIntosh, and L. Spiccia, Miniature inhalation therapy platform using surface acoustic wave microfluidic atomization, *Lab Chip* **9**, 2184 (2009).

[2] A. Rajapaksa, A. Qi, L. Y. Yeo, R. Coppel, and J. R. Friend, Enabling practical surface acoustic wave nebulizer drug delivery via amplitude modulation, *Lab Chip* **14**, 1858 (2014).

[3] A. Winkler, A. Kirchner, P. Bergelt, R. Hühne, and S. Menzel, Thin film deposition based on microacoustic sol atomization (MASA), *J. Sol-gel Sci. Technol.* **78**, 26 (2016).

[4] M. Darmawan, K. Jeon, J. M. Ju, Y. Yamagata, and D. Byun, Deposition of poly(3,4-ethylenedioxythiophene)-poly(styrenesulfonate) (PEDOT-PSS) particles using standing surface acoustic waves and electrostatic deposition method for the rapid fabrication of transparent conductive film, *Sens. Actuators, A* **205**, 177 (2014).

[5] N. Murochi, M. Sugimoto, Y. Matsui, and J. Kondoh, Deposition of thin film using a surface acoustic wave device, *Jpn. J. Appl. Phys.* **46**, 4754 (2007).

[6] L. Monkkonen, J. S. Edgar, D. Winters, S. R. Heron, C. L. Mackay, C. D. Masselon, A. A. Stokes, P. R. Langridge-Smith, and D. R. Goodlett, Screen-printed digital microfluidics combined with surface acoustic wave nebulization for hydrogen-deuterium exchange measurements, *J. Chromatogr., A* **1439**, 161 (2016).

[7] Y. Huang, S. H. Yoon, S. R. Heron, C. D. Masselon, J. S. Edgar, F. Tureček, and D. R. Goodlett, Surface acoustic wave nebulization produces ions with lower internal energy than electrospray ionization, *J. Am. Soc. Mass Spectrom.* **23**, 1062 (2012).

[8] J. Ho, M. K. Tan, D. B. Go, L. Y. Yeo, J. R. Friend, and H.-C. Chang, Paper-based microfluidic surface acoustic wave sample delivery and ionization source for rapid and sensitive ambient mass spectrometry, *Anal. Chem.* **83**, 3260 (2011).

[9] T. Nakamoto, K. Hashimoto, T. Aizawa, and Y. Ariyakul, in *Frequency Control Symposium (FCS), 2014 IEEE International* (2014), p. 1.

[10] M. Kurosawa, T. Watanabe, A. Futami, and T. Higuchi, Surface acoustic wave atomizer, *Sens. Actuators, A* **50**, 69 (1995).

[11] A. Winkler, S. Harazim, D. J. Collins, R. Brünig, H. Schmidt, and S. B. Menzel, Compact SAW aerosol generator, *Biomed. Microdevices* **19**, 9 (2017).

[12] A. Winkler, S. Harazim, S. Menzel, and H. Schmidt, SAW-based fluid atomization using mass-producible chip devices, *Lab Chip* **15**, 3793 (2015).

[13] A. Qi, L. Y. Yeo, and J. R. Friend, Interfacial destabilization and atomization driven by surface acoustic waves, *Phys. Fluids* **20**, 074103 (2008).

[14] D. J. Collins, O. Manor, A. Winkler, H. Schmidt, J. R. Friend, and L. Y. Yeo, Atomization off thin water films generated by high-frequency substrate wave vibrations, *Phys. Rev. E* **86**, 056312 (2012).

[15] W. Thomson, XLVI. hydrokinetic solutions and observations, *London, Edinburgh Dublin Philos. Mag. J. Sci.* **42**, 362 (1871).

[16] R. J. Lang, Ultrasonic atomization of liquids, *J. Acoust. Soc. Am.* **34**, 6 (1962).

[17] A. Winkler, P. Bergelt, L. Hillemann, and S. Menzel, Influence of viscosity in fluid atomization with surface acoustic waves, *Open J. Acoust.* **6**, 23 (2016).

- [18] T. Hirotomto, M. Hara, H. Kuwano, T. Kudo, and H. Kobayashi, in *2015 IEEE International Ultrasonics Symposium (IUS)* (2015), p. 1.
- [19] C. F. Lange and W. H. Finlay, Overcoming the adverse effect of humidity in aerosol delivery via pressurized metered-dose inhalers during mechanical ventilation, *Am. J. Respir. Crit. Care Med.* **161**, 1614 (2000).
- [20] A. R. Martin and W. H. Finlay, The effect of humidity on the size of particles delivered from metered-dose inhalers, *Aerosol Sci. Technol.* **39**, 283 (2005).
- [21] D. Niedermeier, J. Voigtländer, S. Schmalfuß, D. Busch, J. Schumacher, R. A. Shaw, and F. Stratmann, Characterization and first results from LACIS-T: a moist-air wind tunnel to study aerosol-cloud-turbulence interactions, *Atmos. Meas. Tech.* **13**, 2015 (2020).
- [22] See Supplemental Material at <http://link.aps.org/supplemental/10.1103/PhysRevApplied.14.014071> for experimental setup during droplet size measurement using a SAW aerosol generator inside the turbulent moist-air wind tunnel LACIS-T (Leibniz Tropos), Germany, (2020).
- [23] M. Roudini and G. Wozniak, Experimental investigation of spray characteristics of Pre-filming Air-blast atomizers, *J. Appl. Fluid Mech.* **11**, 1455 (2018).
- [24] A. R. Rezk, O. Manor, J. R. Friend, and L. Y. Yeo, Unique fingering instabilities and soliton-like wave propagation in thin acoustowetting films, *Nat. Commun.* **3**, 1167 (2012).
- [25] See Supplemental Material at <http://link.aps.org/supplemental/10.1103/PhysRevApplied.14.014071> for microscopy high-speed video showing the front view on the whole atomization zone at a fluid flow rate of 30 $\mu\text{l}/\text{min}$. Germany, (2020).
- [26] See Supplemental Material at <http://link.aps.org/supplemental/10.1103/PhysRevApplied.14.014071> for microscopy high-speed video showing the front view of the atomization zone at higher magnification and for different liquid flowrates (15, 30 and 50 $\mu\text{l}/\text{min}$). Germany, (2020).
- [27] B. Karri, S.-W. Ohl, E. Klaseboer, C.-D. Ohl, and B. C. Khoo, Jets and sprays arising from a spark-induced oscillating bubble near a plate with a hole, *Phys. Rev. E* **86**, 036309 (2012).
- [28] S. Xiong, L. Chin, K. Ando, T. Tandiono, A. Liu, and C. Ohl, Droplet generation via a single bubble transformation in a nanofluidic channel, *Lab Chip* **15**, 1451 (2015).
- [29] T. F. Hueter and R. H. Bolt, *Sonics: Techniques for the use of Sound and Ultrasound in Engineering and Science* (John Wiley & Sons, Inc., The United States of America, New York, 1955).
- [30] R. E. Apfel and C. K. Holland, Gauging the likelihood of cavitation from short-pulse, low-duty cycle diagnostic ultrasound, *Ultrasound Med. Biol.* **17**, 179 (1991).